Prepublished copy

Nature Environment & Pollution Technology

This is a peer-reviewed prepublished version of the paper to be published in Vol. 25, No. 2, June 2026 issue

Performance Evaluation of Poly Ether Sulfone Nanocomposite Membranes in the Separation of Evans Blue Dye

S. Joy Madhumitha†, P. Jegathambal, S. Devika and C. Mayilswami

Water Institute, Karunya Institute of Technology and Sciences, Coimbatore 641114, Tamil Nadu, India

† Corresponding Author: S. Joy Madhumitha; joymadhumitha@karunya.edu.in

† https://orcid.org/0009-0009-0475-6917

Key Words	Nanocomposite Membranes, Membrane Filtration, Textile industries, Dyes, Polyether sulfone
DOI	https://doi.org/10.46488/NEPT.2026.v25i02.B4370 (DOI will be active only after the final publication of the paper)
Citation for the Paper	Joy Madhumitha, S., Jegathambal, P., Devika, S. and Mayilswami, C., 2026. Performance evaluation of poly ether sulfone nanocomposite membranes in the separation of evans blue dye. *Nature Environment and Pollution Technology*, 25(2), B4370. https://doi.org/10.46488/NEPT.2026.v25i02.B4370

ABSTRACT

The water pollution caused by the textile sector poses significant health and environmental challenges due to the discharge of untreated dye-laden effluents into natural water bodies. Conventional dye removal methods are often cost-prohibitive and energy-intensive. The advancement in Membrane filtration is its scalability, but it exhibits fouling. This research study focuses on preparing cost-effective, eco-friendly membranes and evaluating the performance of PES incorporated inorganic (TiO_2), carbon-based (AC), and green-synthesized, eco-friendly moringa seed extract, it is biosorbents,. Previous research have been done with these nanoparticles separately but in this paper altogether were detailly compared and also the nanocomposite membranes were compared with commercial nanofiltration membrane (CM NF 90). The physical properties of the membranes were evaluated by water uptake, porosity, and mean pore radius. The membrane characterizations are determined using Field Emission Scanning Electron Microscopy (FESEM) and Energy Dispersive X-ray Spectroscopy (EDS), confirming the successful integration of nanomaterials and improvements in membrane morphology. The dead-end filtration system was used to evaluate the performance of the membranes in removing Evans blue dye. It was observed that the Color Removal Efficiency (CRE) of PES/TiO_2, PES/AC, and moringa-based membranes was 97.9%, 92%, and 98.2%. The activated carbon (AC) and titanium dioxide (TiO_2) PES membranes exhibit steady flux. The Moringa-based membrane exhibited a remarkable dye rejection rate and high flux but the flux decreases gradually due to fouling. These results confirm that nanocomposite membranes enhance dye removal efficiency and stability. Therefore, the nanocomposite PES membrane has the potential for the better dye removal and has broad applications in dye reomoval from the waste water from textile industries.

INTRODUCTION

Yale University ranked the Unsafe Drinking Water index of countries; India ranked 141 out of 180 countries (Hossain et al. 2018). The World Bank reported that India 70% of freshwater is contaminated and that 163 million Indians lack safe drinking water. Industrial pollution is the primary cause of water contamination. The textile industry is the major consumer of water, i.e., around 425,000 gallons of fresh water each day (Hossain et al. 2018). It has been reported that around 8,000 different types of synthetic dyes are utilized (Araujo et al. 2010). The dyeing process by itself is responsible for generating 70% of the wastewater flowing into natural streams. The textile industry alone discharges the effluent about 70 billion tons annually (Hossain et al. 2018). Large-scale industries have enormous areas for effluent treatment, but small-scale industries discharge effluent without treatment. The effluent includes toxic chemicals such as ammonia (NH3), phenols, dispersants, leveling agents, salts, carriers, acids, alkalis, color residues, dissolved solids, and large amounts of suspended salts (Madhumitha et al. 2023).

Dye is an intensely colored organic substance. Dye has a chemical structure (R-B-X), where R represents a chromophore group, B denotes the bridging group, and X signifies the reactive group. Most of the 70% of textile dyes are Azo dyes that contain aromatic amines, benzene, and naphthyl (Woo et al. 2016). Azo dyes are more toxic, decrease light penetration, and hinder photosynthesis. They are carcinogenic in nature, impact microbes, and increase the BOD of effluent (eutrophication), which negatively affects aquatic life (Liu et al. 2017). In this study, experimental investigations were carried out using Evans Blue Dye, a water-soluble di-azo synthetic dye, with 0.5 to 2.0 µm-sized dye particles (Wooddell et al. 2011). The chemical structure comprises a di-sodium salt with sulfonated benzene rings linked by azo groups (-N=N-). The Evans blue dye chemical structure is depicted in Figure 1.

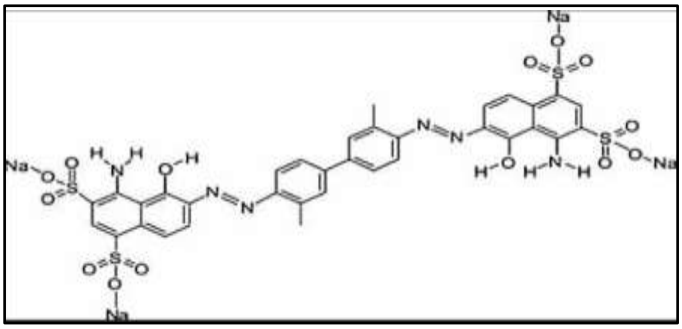

Fig. 1: Evans Blue Dye Chemical Structure

There are various physical, chemical, and biological methods available for the treatment of textile wastewater, as shown in Figure 2 (Aghili et al. 2017). Among these methods, membrane technology provides a sustainable and efficient approach for treating dye effluents, achieving high removal efficiencies that can eliminate over 90% of dyes, including divalent and monovalent molecules (Lin et al. 2019). The membrane filtration has minimal chemical usage, a compact footprint, and offers flexibility in operation. A membrane acts as a selective barrier that permits the passage of certain

constituents while retaining other constituents found in the liquid/gas mixture. Based on size, there were microfiltration, ultrafiltration, nanofiltration, reverse osmosis, and ion exchange membranes, as displayed in Table 1. In this study, the prepared polymer nanocomposite membranes can be identified as ultrafiltration membranes, which are capable of removing dyes at lower applied pressures compared to nanofiltration and reverse osmosis membranes (Moradihamedani 2022).

The literature lacks the use of green synthesis of membranes, and the chemicals are costly when used on a large scale. The membrane technology faces certain challenges, including fouling, which decreases the flux rate and diminishes the economic effectiveness of membranes. The fouling present in the membranes was attributed to the water-repelling interactions between the membrane's top surface and solute particles (Thamaraiselvan et al. 2015). To overcome the limitations of the membranes, several modifications, cross-linking, blending, and doping, have been done (Rahimpour et al. 2008). The pretreatment of the effluent by the activated oxygen process and other processes was done to reduce fouling, and this is an extra time-consuming method (Lin et al. 2019).

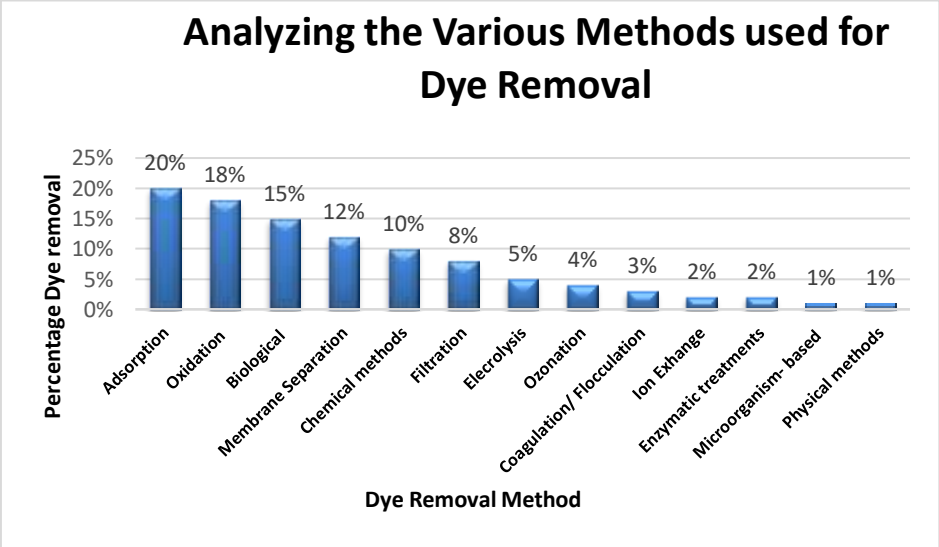

Fig. 2: Literature Review on methods of dye removal

Table 1: Classification of Membranes based on Pore size

Membrane Type	Pore Size	Pressure (bar)	Removes
Micro Filtration (MF)	From 0.1 to 10 µm	0.1-2	Suspended solids, bacteria
Ultra-Filtration (UF)	From 0.01 to 0.1 µm	2-5	Colloids, macromolecules, some dyes
Nano Filtration (NF)	From 0.001 to 0.01 µm	6-20	Divalent ions, small dyes (300-1000 Da)
Reverse Osmosis (RO)	<0.001 µm	15-80	Monovalent ions, all dyes, and salts

This study examined the surface modification of membranes using nanomaterials, including activated carbon, a carbon-based nanomaterial; titanium dioxide, a metal-based nanomaterial; and moringa seed extract, a biosorbent material. The nanomaterials added to the polymer enhance the water uptake capacity of the membranes, consequently improving their workability. In the present research, polyether sulfone (PES) was identified as a high-performance inorganic polymer known for its outstanding mechanical and thermal properties. It was classified as a hydrophobic polymer (Hasani-Sadrabadi et al. 2010). Polyether sulfone possesses the ability to withstand high pH levels and resist acids, alkalis, and organic solvents. Moringa Oleifera seed extract, specifically derived from its seeds, functions as a natural coagulant and adsorbent, facilitating high water recovery and effective contaminant removal (Jayabalakrishnan et al. 2023). The powdered activated carbon with a sieve size of 200 microns (1/5) was identified as a highly porous carbonaceous material that offers a large surface area and antifouling capabilities (Jayabalakrishnan et al. 2023). Titanium dioxide with a particle size below 25 nm, non-toxicity, and affordability, it was widely used. It was effective in degrading organic pollutants and improving antifouling properties (Stawade et al. 2021). Comparing the performance of the prepared membranes with commercial membrane (CM NF 90), that is a nanofiltration membrane. The commercial membranes are costly and prepared with chemicals, which are toxic in nature. This work focus to produce cost-effective, non-toxic and environmental sustainable resources as nanomaterials to improve the dye removal performance in PES polymer membrane.

2. MATERIALS AND METHODS

The reagents utilized for membrane synthesis were of analytical quality and were employed without additional purification. The polymer utilized in this study, polyether sulfone (PES), was sourced from Lobachemie. The organic solvent n-methyl-2-pyrrolidone (NMP, greater than 99. 5% pure) was obtained from Sigma Aldrich. The titanium dioxide nanoparticles (<25 nm) were obtained from Sigma Aldrich (CAS Number: 13463-67-7). The powdered activated carbon with a sieve size of 200 US Mesh (0.075 mm) and a particle size of minus (1/4) was sourced from Activcarb. Moringa seeds were sourced from Rajaangam Industries, Country Drug House, Coimbatore. The feed solution used for filtration was prepared from Evans Blue at 20 ppm (dye content: 86%) obtained from Lobachemie.

2.1 Activated Carbon (AC)

The powdered activated carbon utilized possesses a low volume pore and a large surface area to volume ratio, with a minimal diffusion distance. The AC exhibits a high degree of micro porosity and enhanced adsorption (Lin et al. 2019). The figure displays the SEM image of powdered activated carbon, indicating that the particles possess a uniform pore distribution and flat surface morphology (Lin et al. 2019). Incorporating AC into the polymer solution increases the membrane porosity, with its pore properties detailed in Table 2 and Figure 3. Greater than 0.5 wt% of AC results in agglomeration and membrane roughness. Therefore, 0.5 wt% (25 mg) of AC was selected for optimal results (Aghili et al. 2017). PAC itself is hydrophobic, and when combined with polymer, it enhances its water affinity, improving hydrophilicity (Lin et al. 2019).

Table 2: Pore properties of commercially available activated carbon.

Parameters	Range	Quality Control Standards
Average Pore diameter	2.5 (nm)	ASTM D-2867
Total Ash	Max 5.0	ASTM D-2866
BET Surface Area m^2/g	1500-1800	ASTM D-2862
Apparent Density	0.32-0.36	ASTM D-2854
Ball Pan Hardness	92.0+	ASTM D-3802
pH	9-11	ASTM D-3838

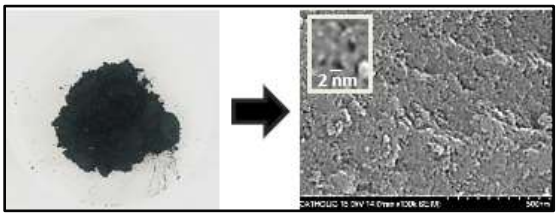

Fig.3: SEM Image of Powdered Activated Carbon [13]

2.2 Titanium Dioxide

Commercially sourced titanium dioxide utilized for the membrane synthesis is a white, amorphous solid, non-combustible and odorless powder which possesses a particle size ranging from 21nm to less than 100 nm, as shown in Figure 4. The chemical composition of TiO_2 is: titanium 59.95% and oxygen 40.05%, with a molecular weight of 79.87 Da. TiO_2 has a relative density of 4.26 g/cm^3 at 25°C, and photocatalytic properties, which aid in degrading organic contaminants, prevent membrane fouling, and improve the efficiency of water permeability (Hossain et al. 2018). The blend of TiO_2 with PES increases the porosity, increases the lengths of micro voids, and decreases the top layer thickness (Shi et al. 2013). TiO_2 has a natural pore-forming property and improves the hydrophilicity (Shi et al. 2013). It also improves the flux, permeability, and has antifouling properties (Hossain et al. 2018).

Fig. 4: SEM Image of Titanium dioxide (Ho 2023)

2.3 Moringa Oleifera Seeds

The moringa seed extract was green synthesized by mixing 10g of moringa seed powder with 100 ml of NMP in a 1:10 ratio, which was then stirred for 2 hours. The prepared moringa seed extract was filtered using normal filter paper. The filtered solution was used for membrane synthesis. To investigate the characteristics of moringa seeds, dried moringa seed nanoparticles were necessary (Jahan et al. 2018). The moringa seed extract includes tiny nanoparticles of a natural coagulant, consisting of protein molecules dispersed in the extracted solution. The excess solution was eliminated by filtering it through filter paper, and the settled particles in the petri dish were allowed to dry in a hot-air oven. The synthesized moringa nanoparticles were analyzed using a field scanning electron microscope, obtaining a mean area of the particles of 150 nm, a perimeter of 120 nm, Ferret diameter of 45 nm, which is the particle size of the moringa particles, as illustrated in Figure 5. From the figure, the morphology was assessed as a heterogeneous distribution featuring a porous matrix. The existence of protein structures creates greater spaces surrounding each particle, enhancing ion adsorption and hydrophilicity. It was observed from the examined morphological profile that moringa seed nanoparticles can function as biosorbents for ion adsorption in membranes.

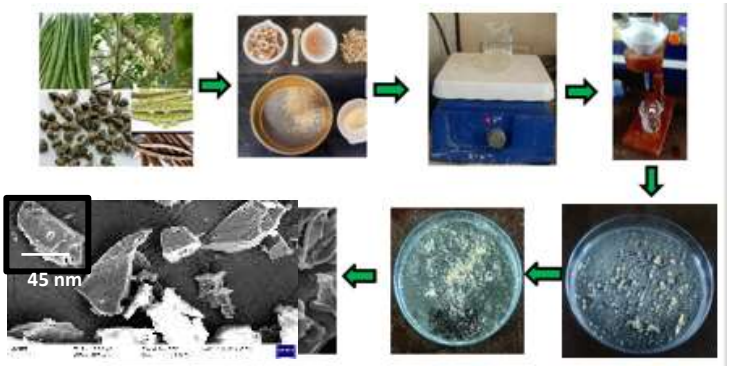

Fig. 5: Preparation of Moringa Seed extract and its SEM image

2.4 Synthesis of PES Nanocomposite Membrane

Polyether Sulfone (PES) is a hydrophobic polymer and has to be therefore has to be dissolved in organic solvents. A 12 wt% solution of Poly Ether Sulfone polymer was dissolved in N-methyl-2-pyrrolidone with (12 wt PES:18 wt NMP) (Xu et al. 2004). The polymer solution was prepared with an organic solvent and mixed in a magnetic stirrer for 6 hours until a clear solution was achieved. The PES control membrane was created as depicted in Figure 3. The nanocomposite membranes were prepared by dispersion and solution blending. To fabricate the PES/TiO_2 nanocomposite membrane (0.1 wt%), 25 mg of TiO_2 nanoparticles was dispersed in a prepared 20 ml of PES polymer solution (Lincy et al. 2020). The polymer solution was stirred

for 8 hours to ensure the uniform dispersion of the nanoparticles. Figure 3 shows the preparation of PES/TiO_2 (Yam et al. 2024). The PES/AC nanocomposite membrane was fabricated by dispersing 25 mg of powdered activated Carbon (0.1 wt%) into the PES polymeric solution (Woo et al. 2011), which was then allowed to get uniform dispersion in a magnetic stirrer for 8 hours (Ho et al. 2018). The PES/Moringa membrane was fabricated with 12 wt% of PES polymer powder incorporated into the filtered moringa extract solution (Almairas et al. 2025). The polymer and moringa nanoparticles were allowed to mix well in the magnetic stirrer for 8 hours to form strong chemical bonds (Nisha et al. 2017). The PES/Moringa polymer solution was thus prepared. The prepared polymer solutions in the individual beakers were placed in the ultra-sonication for thirty minutes to eliminate trapped bubbles and to maintain uniform dispersion. Once the bubbles vanished, the solution was poured onto a petri dish to create a thin film the thickness maintained from 0.3 mm to 0.1 mm. After 2 minutes, it was immersed in the deionized water for interfacial polymerization (Xu et al. 2004). The produced membranes were placed in the deionized water for 24 hours, as displayed in figure 6. Following this, the soaked membranes were removed, dried in the oven, and then stored.

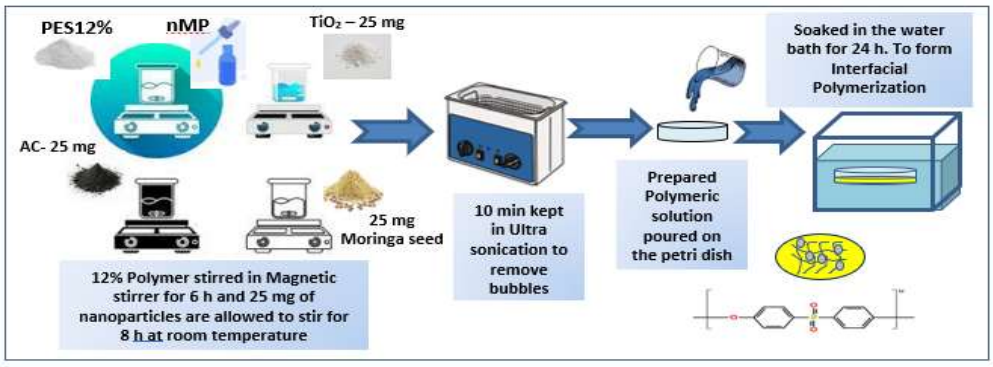

Fig. 6: Synthesis of Nanocomposite Membranes

2.5 Commercial Nano Filtration Membrane

In this study, the performance of the fabricated PES nanocomposite membranes were compared with the commercial nanofiltration membrane, DOW NF 90. The DOW NF 90 (Nanofiltration Membrane), illustrated in Figure 4, from DOW Water and Process Solutions is a high-efficiency water filtration membrane, capable of effectively removing a wide range of contaminants while allowing beneficial minerals to remain (Ehsani et al. 2020). This membrane is outstanding at rejecting organic substances and both divalent and polyvalent ions, making it suitable for applications such as drinking water purification, industrial water treatment, and wastewater recycling. Known for its strength and dependability in difficult settings, the DOW NF 90 membrane significantly contributes to the advancement of sustainable water management practices (Ehsani et al. 2020).

Fig. 7: Membranes used for Filtration

2.6 Characterization of Dye

According to the Indian Standards IS 9508:1980 (Table 6), the discharge standards for dye effluent from a cotton textile mill are: pH 6.7 and 11.8 and, Total Dissolved Salts (mg/l) 1200 to 4438 mg/l. The feed solution utilized for the experiment was synthetic di-azo dye Evans blue has a molecular weight of 961 Da, and dissolves in water at a rate of 280 g/l (Vergis et al. 2019). It has been reported that Azo dyes account for 80% of dyeing processes (El-Sabban et al. 2023). The Evans blue dye, also referred to as T-1824 or Direct Blue 53, is an anionic complex dye with the chemical structure that consists of dimethyl group of 6,6'[(3,3'-Dimethyl[1,1'-biphenyl]-4,4'-diyl) bi (azo)] bis[4-amino-5-hydroxy]-1,3 naphthalene disulfonic acid, tetrasodium salt (She et al. 2008). Due to its high-water solubility, permeability, slow excretion, and strong binding, Evans blue dye requires more attention for treatment (Yao et al. 2018). The sample collected showed a pH that was almost neutral, and the Total Dissolved Solids (TDS) of the nanocomposite membranes were 40% higher than those of PES control membranes, as demonstrated in table 3.

Table 3: Water Quality parameters of the Sample

Tested Water Sample	pH	TDS (mg/l)
Evans Blue (20 PPM)	8.22	159
Distilled water used for dye preparation	7.58	1
PES control	7.77	53
PES TiO2	7.78	33
PES Moringa	7.92	36
PES/AC	7.87	34

3 MEMBRANE CHARACTERIZATION

3.1 FESEM with EDS

The surface structure of the membranes was analyzed by Field Scanning Electron Microscope (FESEM). The pore and particle size were measured on the top of the surface and the cross-sectional

morphology of the membrane. The surface images were analyzed using FESEM integrated with Energy Dispersive X-Ray Spectroscopy (EDS) (Sigma HV – Carl Zeiss of Bruker Quantax 200 –Z10 EDS Detector). The elemental composition of the membrane was evaluated using the EDS. The prepared membranes were cut into small pieces of 1x 1 cm and cleaned. To get effective scanning, the membranes were immersed in liquid nitrogen to freeze the pores for 60 to 90 seconds. Frozen membrane fragments were kept in the air for drying. To have electrical conductivity, the fragments were gold sputtered and viewed with the microscope at 15-20 kV.

3.2 X-ray diffraction

The crystallinities of the Polyether Sulfone control and fabricated composite membranes were tested with an X-ray diffraction instrument (Shimadzu XRD-6000, Japan) with Cu, Kα Cr radial, Ni filter, X=0.154 nm, scan range: 2θ = 5-80^{o}, and scan step = 10^{o}/0.6 s with continuous scan mode. Then the crystallinities were calculated using Bragg's law.

3.3 Porosity and Pore Size

The percentage of porosity and mean pore size were determined using specific equations. The distribution of membrane pores was determined using equation (1). Here, w_w represents the wet weight of the membrane in grams, and w_d denotes the dry weight of the membrane. The area of the membrane is measured in square centimeters (cm^2) and thickness (t) measured with micro meter converted to cm. ρ_{water} is the density of water (0.998 g/cm^3) at room temperature (Almarzoogi et al. 2016). The values obtained were displayed in Figures 11 and 12.

$$\text{Porosity (\%)} = \frac{\text{Ww}-\text{Wd}}{\rho_{water}} \text{ X } \frac{1}{\pi R^2 t} \text{ X 100 \%} \quad \ldots (1)$$

The membrane pore formation radius is equal to the minimum size of retained impermeable solute (Thamaraiselvan et al.). In order to analyze the size of a membrane's mean pore radius (γ_m) the Guerout- Elfort – Ferry Equation (2) was used (Bae et al. 2022), from the flux and porosity data.

$$\gamma_m = \sqrt{\frac{(2.9-1.75\varepsilon) X\ 8\eta t Q}{\varepsilon X A X \Delta P}} \quad \ldots (2)$$

where η represents the viscosity of water (8.9 X 10^{-4} pa. s), ε signifies the membrane porosity, Q = Permeate volume per unit time (m^3/s), t = membrane thickness (m), A = area of the membrane (m^2), and ΔP denotes the operating pressure (0.8 MPa).

3.4 Water Uptake Test

The hydrophilicity and performance of the membranes were evaluated through the Water Uptake Test. The water absorption was determined by recording their weights before and after being submerged in deionized

water for 24 hours, following the method outlined (Duan et al. 2013). The water absorption capacity was calculate using equation 3.

$$\text{WC (\%)} = \frac{m_w - m_d}{m_d} \text{X100} \quad \ldots (3)$$

3.5 FTIR

Fourier-transform infrared (FTIR) spectroscopy was analyzed using the Shimadzu Prestige 20 IR Spectrometer, based on the principle that molecular bonds absorb specific IR frequencies corresponding to their vibrational transitions. When a broad-spectrum IR beam passes through a sample, each chemical bond that changes in dipole moment absorbs at a distinctive wavelength, producing a spectrum that acts like a molecular "fingerprint." Central to FTIR instrumentation is the Michelson interferometer, which splits and recombines the IR beam using fixed and moving mirrors to generate an interferogram containing all absorbance information. This time-domain signal is digitally converted into a frequency-domain IR spectrum via a Fourier transform, yielding high-resolution, full-spectrum data that almost instantaneously identifies functional groups and materials

3.6 Permeation test:

The permeate flux and fouling test for the prepared membranes were carried out in a dead-end stirrer cell (270 ml) with a membrane surface area of 15.7 cm^2. The laminar flow of the liquid forced inside the membrane of the stirrer cell with a fitted pressure gauge was pressurized with nitrogen gas. The distilled water used as the feed solution was stirred at a rate of 200 rpm. The membrane was soaked in the distilled water for 10 minutes before testing. The membrane was pressurized at minimum 8 bar for an hour and tested at maximum 14 bar for an hour. The pure water flux J_w ($l/m^2.h$) was calculated by the following equation (4):

$$J_w = \frac{V}{A.\Delta t} \quad \ldots (4)$$

Where V is the volume of the permeate pure water (l), A is the membrane effective area (m^2) and Δt is the permeation time (h). The experiments were carried out at room temperature.

3.7 Analysis of Membrane Fouling:

After the pure water flux tests, the dye removal test was carried out by rapidly refilling the 20ppm concentrated Evans blue dye. The dye solution flux J_P (l/m^2h) was measured at 8 bar and 14 bar of two different pressure for an hour based on the permeating water quantity. The flux recovery (FR) was calculated as following equation (5) (Vatanpour et.al. 2012).

$$\text{FR (\%)} = \frac{J_D}{J_P} \text{ X 100} \quad \ldots (5)$$

From FR value, the antifouling property of the membrane was determined. A higher FR value antifouling property of the membrane will be better. Fouling is the resistance formed due to the dye particles deposited on the pores or surfaces or adsorbed onto the membranes. The total fouling ratio (Rt) was defined and calculated using formula (6) (Wu et.al. 2019).

$$Rt\ (\%) = \left(1 - \frac{J_D}{J_W}\right) X\ 100 \qquad \ldots (6)$$

Here, Rt was the ratio of total flux caused by total fouling. The dye rejection of the filtered samples was analyzed using Jasco 600 UV vis Spectrophotometry. The rejection, R, may be computed using the subsequent expression, where C_1 is the feed concentration and C_2 is the permeate concentration, as indicated in equation 7(Jayabalakrishnan et al. 2023).

$$R = \frac{C_1 - C_2}{C_1} x\ 100\ \% \qquad \ldots (7)$$

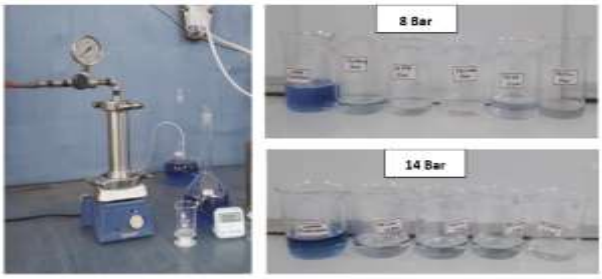

Fig. 8: Dead End Stirrer Cell and Filtered Samples

4 Results and Discussion

4.1 Membrane Morphology and Elemental Analysis

The membrane morphology determined by FESEM at 50kx magnification was analyzed by Image J. The FESEM analysis of PES, PES/TiO_2, and CM NF 90 before and after is shown in Figure 9. The FESEM image of the CM NF 90 membrane before filtration, as shown in Figure 9 (i), depicts a homogeneous mix with good dispersion, indicated by spherical-shaped particles with an average pore size of 6 nm, a diameter of 5.3 nm, and a ferret radius of 3.6 nm for the nanofiltration membrane. The surface morphology was rough with visible cracks, and minimal agglomeration was observed, indicating good dispersion. The asymmetrical particle distribution occurs due to the phase inversion method of membrane preparation. The CM NF 90, after filtration as shown in Figure 9 (j), displays that a filtration cake layer formed due to the rejection of dye particles after filtration with a mean pore size of 19.3 nm, and ferret radius of 2.6 nm decreased by 12%. From the FESEM image of the fabricated PES-control membrane, as shown in Figure 9 (a), it was observed that, the membrane pores were spherical with an average pore size of 8 nm, a ferret radius of 4.2 nm. The surface morphology was smooth with visible pores and no visible cracks or defects. Minimal agglomeration was observed, indicating good dispersion (Gosavi et al. 2014). The particles were arranged uniformly within the PES membrane. In Figure 9(b), the flaky nature of the particles with circular shapes indicates dye rejection.

PES/TiO_2 membrane shows that the pores become narrower in the nanocomposite membrane, leading to a reduction in pore size. Figure 9(d) shows that the PES/TiO_2 membrane has a smooth surface morphology, with a minimum number of pores and a pore size of 4 nm and a ferret radius of 2.4 nm.

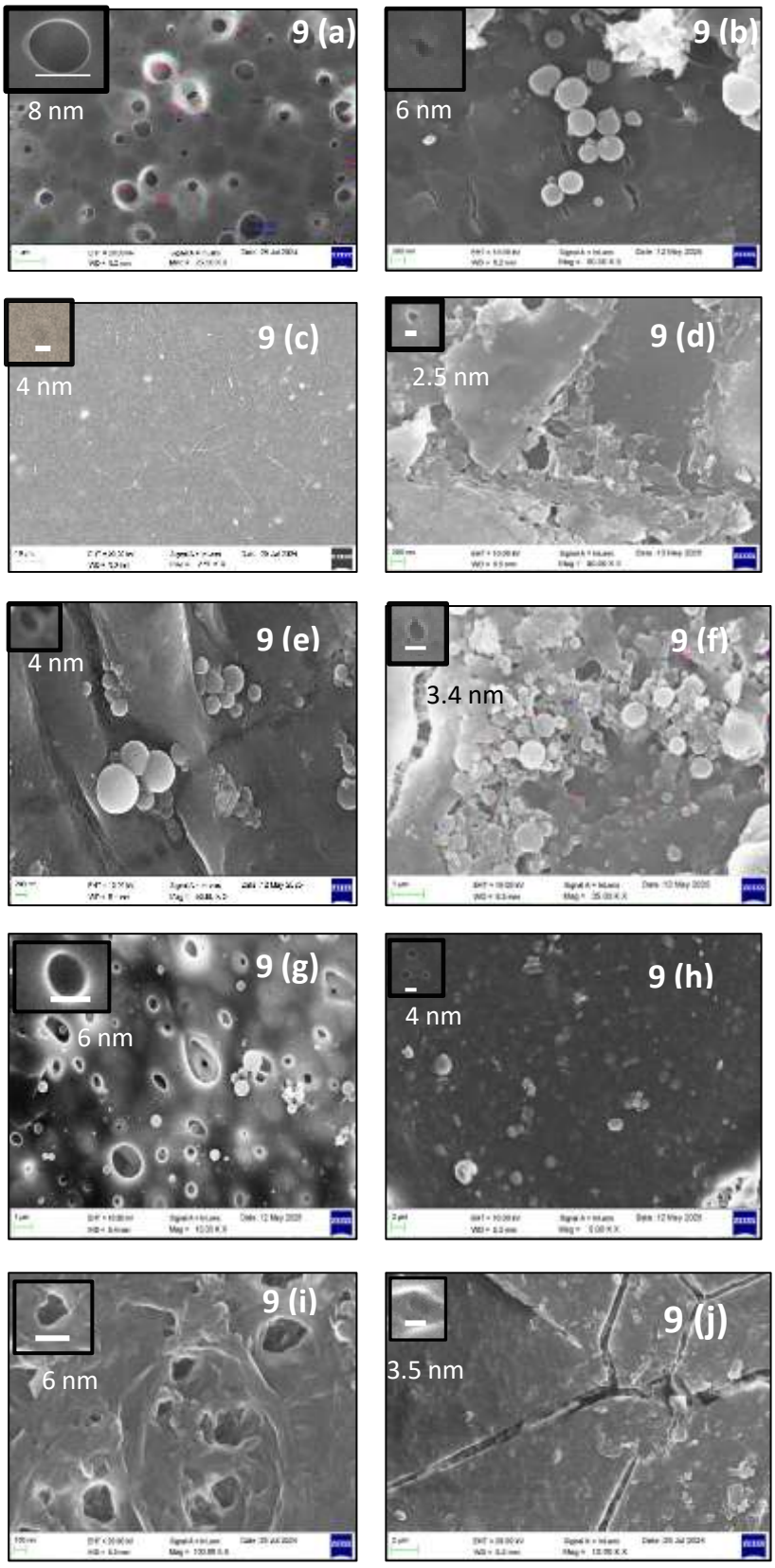

Fig. 9: FESEM Image of (a) PES control before filtration, (b) PES control after filtration, (c) PES TiO_2 before filtration, (d) PES TiO_2 after filtration, (e) PES moringa before filtration, (f) PES moringa after filtration, (g) PES AC before filtration, (h) PES AC after filtration, (i) CM NF 90 before filtration, (j) CM NF 90 after filtration.

The minimal amount of TiO_2 was irreversibly deposited on the membrane surface. After the filtration, the size of the pores was reduced to 2.5 nm due to the dye particles deposited on the inner layer of the pores. The FESEM images of PES moringa membrane before and after filtration are shown in Figures 9 (e) and 9(f), with the obtained pore sizes being 4 nm and 3.4 nm, respectively. The pores of the PES moringa membrane were elongated, and after filtration, increased biofouling was observed. The FESEM images of the PES activated carbon membrane before and after filtration are shown in Figures 9 (g) and 9 (h), which display the round pores with sizes of 6 nm and 4 nm, respectively.

Table 4: EDX Results of Membranes used

Elements	**Atomic weight Percentage**				
	CM NF 90	PES	PES/ TiO_2	PES/Moringa	PES/AC
Carbon	78.35 %	71.18 %	74.12 %	73.00%	72.40%
Oxygen	19.08 %	20.87 %	19.88 %	22.54 %	20.51%
Sulfur	2.57 %	5.24 %	5.30 %	3.69 %	4.98%
Nitrogen	-	2.72 %	-	0.70%	2.10 %
TiO_2	-	-	0.70 %		

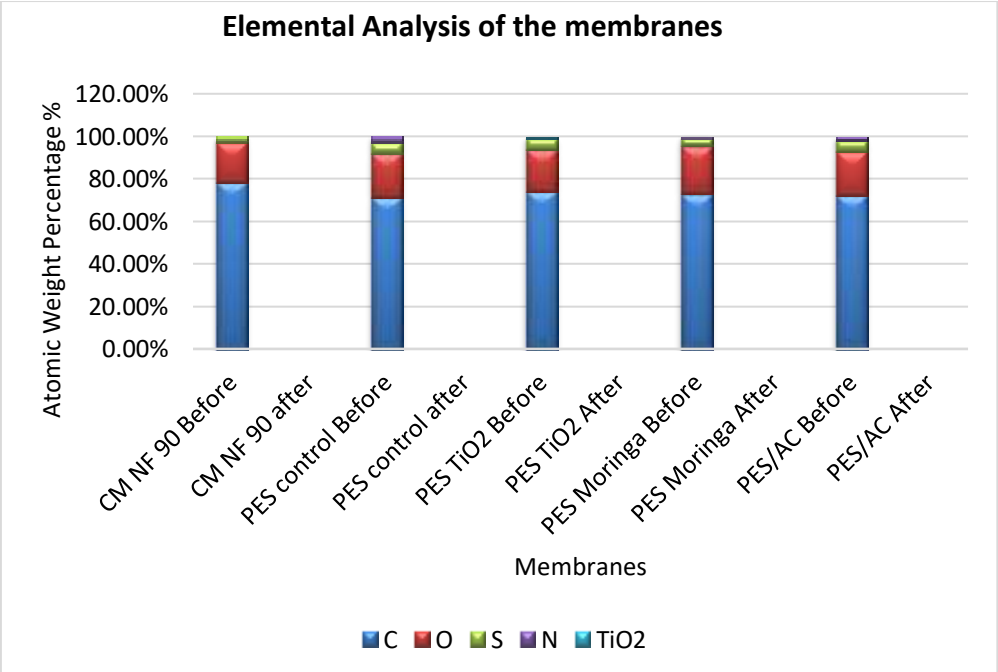

Fig. 10: Elemental analysis of the membranes

The elemental composition of the membrane samples, CM NF 90, PES, and PES/TiO_2, was examined using Energy Dispersive X-Ray Spectroscopy (EDS), as illustrated in Figure 10 and Table 4. Among the detected elements, carbon was the most prevalent, with concentrations of 78.35% in CM NF 90, 71.18% in PES, and 74.12% in PES/TiO_2. Oxygen levels remained relatively uniform across the samples, ranging between 19.08% and 20.87%. A noticeable rise in sulfur content was observed in the PES and PES/TiO_2 membranes (both exceeding 5%) compared to CM NF 90 (2.57%), which may be attributed to the sulfonyl groups. Nitrogen appeared exclusively in the PES membrane at 2.72%, indicating the presence of nitrogen-containing functional groups. Notably, titanium dioxide was present only in the PES/TiO_2 sample at 0.70%, confirming the effective incorporation of TiO_2 nanoparticles. The carbon, oxygen, and sulfur groups are present due to the chemical composition of Polyether Sulfone polymers. These findings affirm the distinct elemental makeup of each membrane, highlighting their unique structural and functional characteristics.

4.2 FTIR

FTIR analysis was used to study how different PES membranes interact with Evans Blue dye and how well they remove it, as shown in Figure 11. The original dye showed specific peaks at 3639 cm^{-1} and 3186 cm^{-1} (O–H or N–H groups), 2353 cm^{-1} (C≡N or CO_2), 1635 cm^{-1} (aromatic rings or C=O groups), and 765 cm^{-1} (aromatic C–H bending). These peaks confirm the presence of sulfonic acid, amine, and aromatic structures in the dye. When the dye interacted with the membranes, some peaks weakened or disappeared. This change was most noticeable in the PES TiO_2 and PES AC membranes, showing that these membranes effectively removed the dye. PES AC strongly reduced the 2353 and 1635 cm^{-1} peaks, confirming that it could adsorb nitrogen and aromatic parts of the dye. PES TiO_2 almost completely removed all major peaks, showing that it can break down the dye. The FTIR peaks indicative of protein-based functional groups (amide, hydroxyl) suggest that bioactive compounds from Moringa oleifera (e.g., cationic proteins, polyphenols) interact with the polymer matrix via hydrogen bonding and electrostatic forces, enhancing hydrophilicity and dye adsorption. The PES Moringa and CM NF 90 membranes exhibited some dye removal, although not as much as the others. The PES control membrane exhibited minimal change, indicating that it removed less dye (Safarpour et al. 2016). Thus, modifying the membrane, especially with TiO_2 or activated carbon, improved its dye removal ability.

Table 5: Major Observed Peaks and Corresponding Functional Groups

Peak (cm^{-1})	Functional Group	Typical Vibration Mode
3639.675	O–H or N–H stretch (free OH)	Stretching
3186.4	N–H or O–H (hydrogen-bonded)	Stretching
2353.155	C≡N, C≡C, or CO_2 asymmetric stretch	Stretching
1635.63	C=C (aromatic), C=O (amide I) or N–H bend	Stretching / bending

765.739	C–H (aromatic out-of-plane bending)	Bending

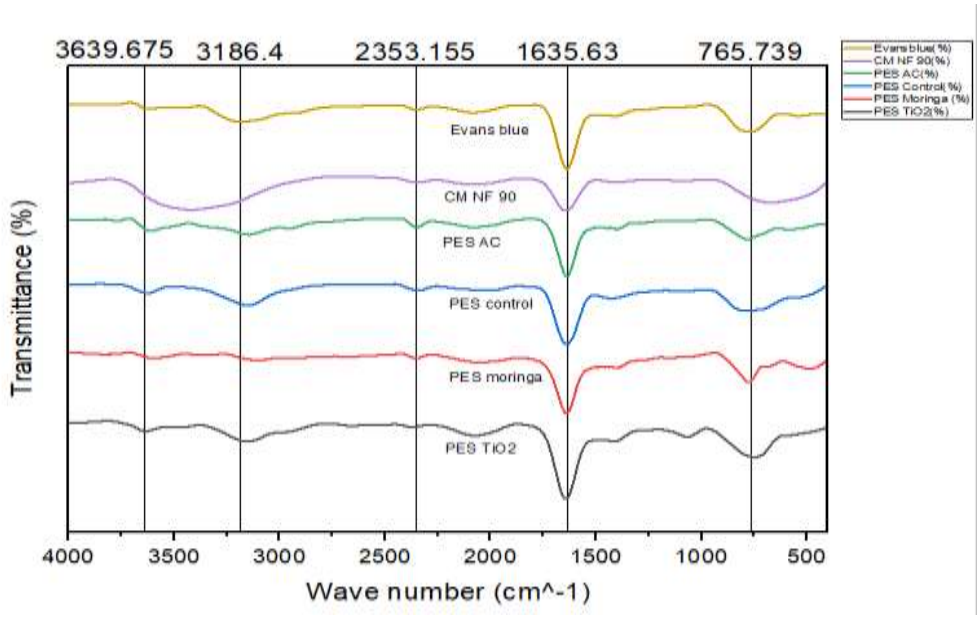

Fig.11: FTIR spectra of permeate water from the membranes used

4.3 Surface Characterization of the membranes

Membrane porosity was determined using Equation (2), which calculates the ratio of the wet weight and dry weight of the membrane to the water's density and the membrane's geometric parameters (Almarzoogi et al. 2016). As shown in Figure 13, the porosity was greatly affected by the type of nanoparticle incorporated during membrane preparation. The CM NF90 membrane demonstrated a porosity of 43.68%, aligning with its typical nanofiltration structure characterized by compact pores. In contrast, the unmodified PES control membrane displayed a porosity of 14.93%. A notable increase to 47.49% was observed with the addition of TiO_2. TiO_2 acts as a pore-inducing agent, enhancing the membrane's porous nature through accelerated phase separation (She et al. 2008). On the other hand, incorporating Moringa and activated carbon (AC) led to reduced porosity values of 76.35% and 61.22%, respectively. This decline may be due to larger pore radius as shown in figure 11 (Thamarai selvan et al. 2015).

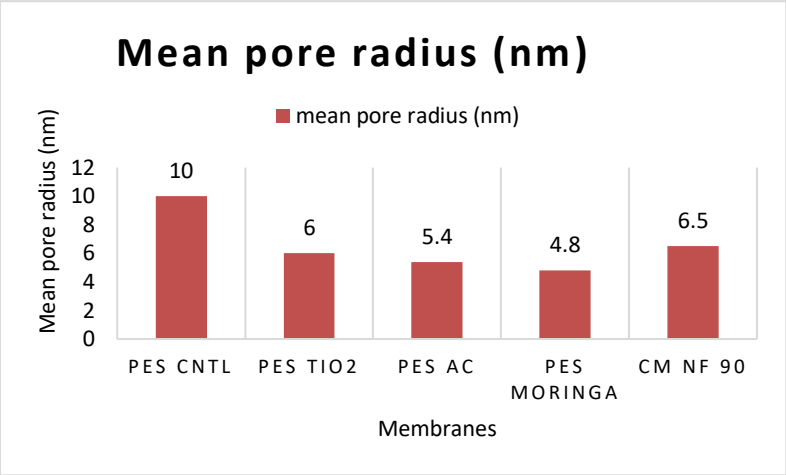

Fig. 12: Mean pore radius of membranes

Guerout–Elford–Ferry equation was used to determine the mean pore radius (γ_m), influences the parameters such as water viscosity, membrane porosity, thickness, and the applied pressure. This method enables the estimation of pore size based on dye permeability. According to Figure 12, the CM NF90 membrane had the smallest mean pore radius of 6.5 nm, reflecting its dense structure and suitability for nanofiltration applications. The PES control sample showed a larger γ_m of 10 nm. The addition of TiO_2 resulted in a slight decrease in pore radius to 6 nm, indicating the formation of more consistent, slightly smaller pores attributed to the role of TiO_2 in enhancing pore generation. On the other hand, modifications with Moringa and activated carbon (AC) led to significantly larger mean pore radii of 4.8 nm and 5.4 nm, respectively, suggesting a looser and more open pore formation. These observations demonstrate the impact of various additives on membrane pore development, with TiO_2 contributing to both higher porosity and relatively well-regulated pore size.

The determined mean pore radius with volume of flow using the Guerout–Elford–Ferry equation was nearly the same as the FESEM pore size values. The PES membrane itself has good porosity, mean pore size, and water uptake capacity. The pore size of moringa and activated carbon incorporated membranes increases due to the larger surface area of nanoparticles. These nanomaterials opened more bonding sites. The pore sizes of the titanium incorporated membranes have no visible pores, as observed in the FESEM image in Figure 9(d). The stable structure of titanium nanoparticles resulted in a smaller pore size; therefore, porosity is higher, as observed in Figure 13. The commercial membrane has an average pore size, porosity, and water uptake capacity, as observed in Figures 12 and 13.

The water uptake capacity value was determined using Equation (3), which calculates the water content (WC%) based on the percentage increase in membrane mass due to water uptake. As shown in Figure 13, the data highlight how the presence of various additives affects the membranes' affinity for water. Nanocomposite membranes, especially those modified with Moringa seed extract and activated carbon (AC), demonstrated a significantly greater capacity to absorb water compared to the control membrane. The water

uptake capacity of the nanocomposite membrane has an increased affinity for water. The water uptake capacity decreases with fewer function groups and bonding sites.

This suggests an enhancement in hydrophilic properties, which were essential for improved water transport and reduced fouling. In particular, PES membrane with Moringa has 530% and AC has 87.50 % water uptake capacity, showing about an increase in water absorption relative to the PES control of 80%. The PES/TiO_2 has 266.67% of water uptake capacity, which is slightly higher than the PES control. The CM NF 90 commercial membrane has 57.14% water uptake capacity, which is very low compared to other membranes. The natural and carbon-based additives can increase surface hydrophilicity or roughness, thereby promoting higher water uptake. Integrating bio-derived and nanomaterial additives can significantly enhance membrane-water interactions and overall functional performance.

From the porosity, the membrane permeability was determined, and from the water uptake capacity, the hydrophobic nature of the PES membrane rate enhanced through nanomaterials. The PES membrane has good water uptake capacity with average porosity. The Porosity of titanium dioxide was higher due to its stable structure, which provides very small pores in the membranes. Titanium dioxide was hydrophobic; therefore, it has an average water uptake capacity. PES moringa has a large pore size; therefore, the porosity of the moringa incorporated membrane was very less. Moringa was a natural biosorbent; hence, the water uptake capacity was very high. Similar to moringa, activated carbon is an adsorbent with high porosity, and high water uptake capacity.

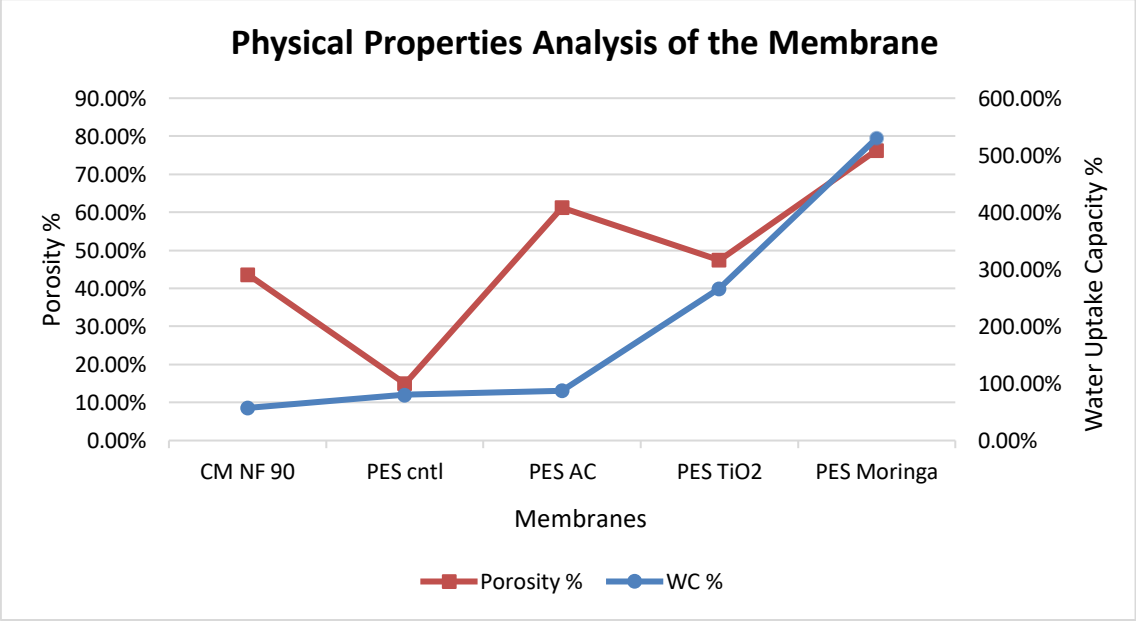

Fig. 13: Water Uptake Capacity, Porosity curve of membranes

4.4 Permeation Test

The dye rejection flux determined for the prepared membranes for 8 and 14 bars pressure for 60 minutes (1 hour). The PES membrane has a flux of 27 l/m^{2}h and 38 l/m^{2}h, PES/TiO_2 has flux of 44 l/m^{2}h and 91 l/m^{2}h, PES/ AC has an average flux of 59 l/m^{2}h and 88 l/m^{2}h, PES/moringa has a flux of 88 l/m^{2}h and 147 l/m^{2}h, CMNF 90 has a flux 13 and 31 l/m^{2}h respectively, as shown in Figure 14. The dye water of 20 ppm concentration, permeability of PES nanocomposite membrane, assessed using Dead End Filtration as illustrated in Figure 8 (Woo et al. 2016). Further comparison revealed differing performance mechanisms between PES/Moringa and PES/AC membranes, though both improved permeability. The PES/Moringa membrane produced a steady but moderate permeate, demonstrating moringa's role as a natural coagulant that helps in pollutant removal by adsorption and flocculation (Duan et al. 2013). Although it was slightly less effective in terms of flux compared to PES/AC. Over extended operation, all membrane types experienced a gradual decline in permeate volume, a typical result of membrane fouling in pressure-driven systems (Woo et al. 2016). The commercial NF90 membrane consistently showed lower permeate volumes than its modified PES counterparts, highlighting the performance improvements achieved through nanocomposite enhancements. Overall, the findings indicate that incorporating materials like AC and TiO_2 not only improves initial membrane permeability but also contributes to better fouling resistance and sustained filtration performance under varying operational conditions.

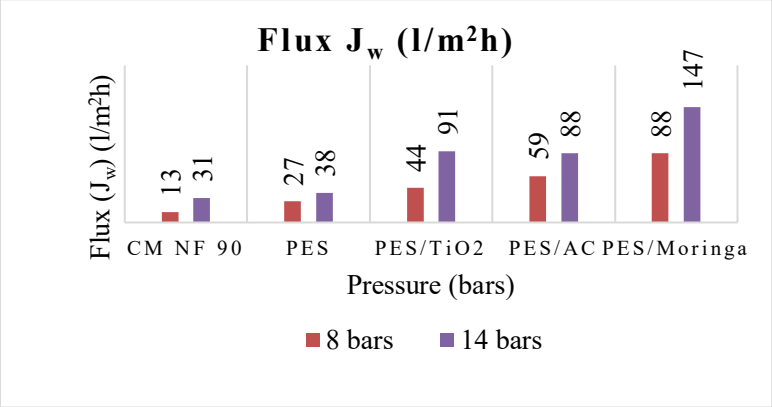

Fig. 14: Membrane Pure Water Flux at 8 and 14 bars

The permeability of PES-based nanocomposite membranes was examined using a Dead-end Filtration system, as illustrated in Figures 15 and 16, with rejection rates determined by Equation (4) (Jayabalakrishnan et al. 2023). The tests involved filtering a 20 ppm Evans Blue dye solution and showed that additives like titanium dioxide (TiO_2), Moringa seed extract, and activated carbon (AC) had a notable impact on membrane performance. Among them, PES/AC and PES/TiO_2 membranes exhibited superior permeability during the early stages of filtration. This enhancement is attributed to their elevated porosity and hydrophilic nature characteristics that promote higher water flux, as previously reported (AlMarzoogi et al. 2016). PES/AC, in particular, achieved the highest initial permeate volume (60 ml at 10 minutes under 14 bar), a result linked to activated carbon's extensive surface area and its ability to adsorb organic contaminants, thus minimizing

fouling (Bae et al. 2022). Likewise, PES/TiO_2 showed strong initial permeability due to improved pore development during synthesis, in agreement with observations (Shi et al. 2013). However, the PES/TiO_2 membrane's flux declined over time, likely a result of its greater affinity for dye molecules, leading to faster fouling on the membrane surface.

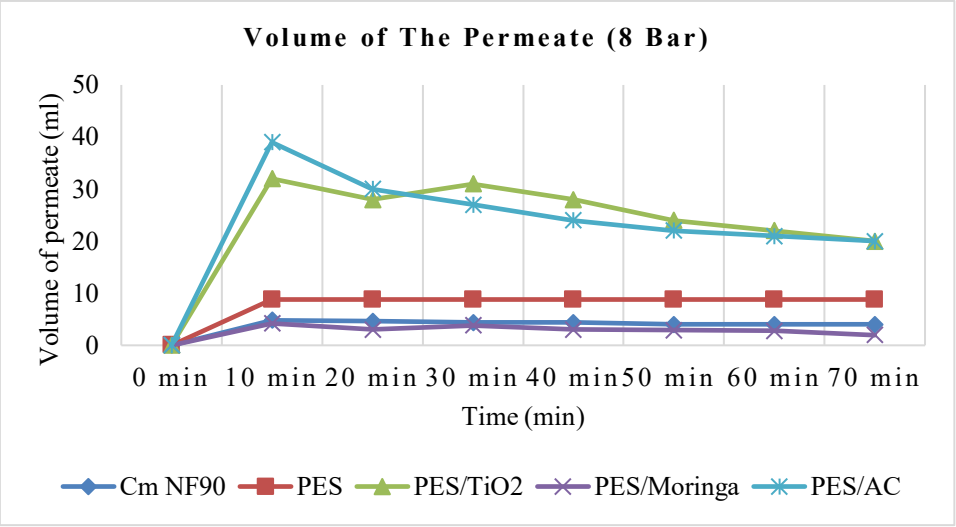

Fig.15: Graphical Representation of Volume of Permeate at 8 bars

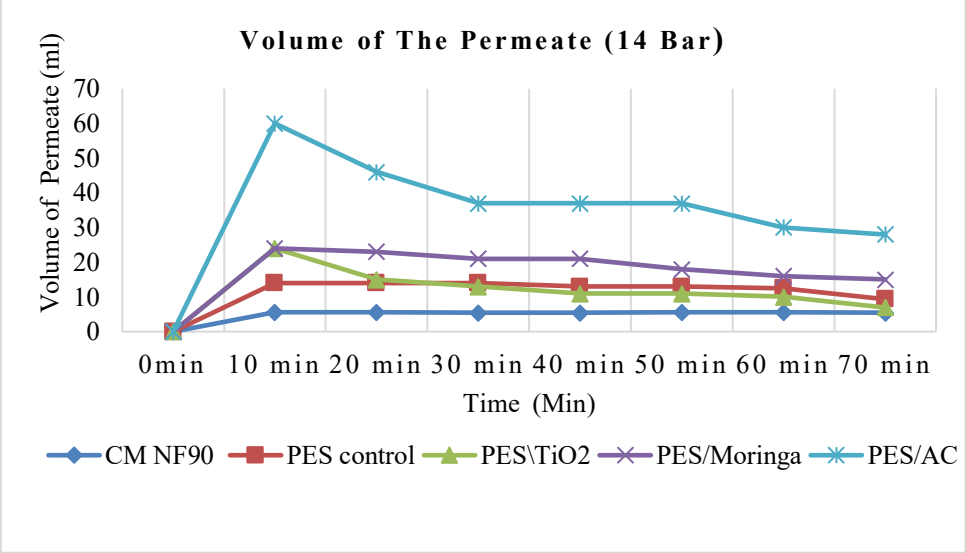

Fig. 16: Graphical Representation of Volume of Permeate at 14 bars

The PES membrane has good permeability, but to improve the flux at low operating pressure, nanomaterials were incorporated. PES with AC has increased permeability because of the greater water uptake capacity and porosity of PES/AC membranes more water uptake capacity and porosity, making the membrane more hydrophilic for the filtration process, However, the deposition of dye particles on the hydrophilic membrane due to van dar waals interactions caused the flux to keep reducing, resulting in fouling. Next to the activated carbon, the titanium dioxide-incorporated membrane has greater permeability. The titanium dioxide has porosity; it increases permeability. Due to the clogging of small pores on the membrane, the flux kept

decreasing. The moringa-incorporated membrane has a large pore size and good water uptake capacity; hence, the moringa-incorporated membrane has a stable flux.

4.6 Anti-fouling Characterization of the membranes

The dye rejection flux was determined for the prepared membranes for 8 and 14 bars pressure for 60 minutes (1 hour). The PES membrane has a flux of 24 l/m^{2}h and 37 l/m^{2}h, PES/TiO_2 has flux of 41 l/m^{2}h and 81 l/m^{2}h, PES/ AC has an average flux of 10 l/m^{2}h and 60 l/m^{2}h, PES/moringa has a flux of 79 l/m^{2}h and 121 l/m^{2}h, CMNF 90 has a flux 12 and 17 l/m^{2}h respectively, as shown in Figure 17.

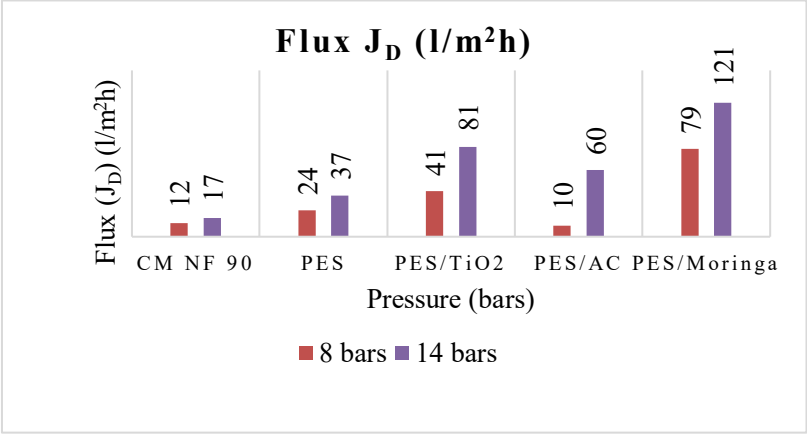

Fig. 17: Membrane Dye Water Flux at 8 and 14 bars

The dye water flux exhibited low value, when compared with pure water flux figure 14. The decline in the flux caused by dye particles settled on the pores and resulted in fouling. The continuous dye particle deposition results in cake formation. If the operating pressure increases, the flux also increased. The more pressure can allow the large volume of liquid to pass through. From figure 18, the Flux Recovery (FR) is the anti-fouling property of the membrane. All the membranes except PES moringa has more than 80% Flux recovery and exhibit better anti-fouling properties. Hence, Flux recovery is less compared with other membranes. From the figure 17, PES moringa and Cm NF 90 nanofiltration membranes produced more total fouling Ratio (Rt) than other nanocomposite membranes. The PES moringa (bio-composite) membrane, that has more water uptake capacity and more affinity towards the dye solution that leads to more fouling and low anti-fouling properties. The nanofiltration membrane CM NF 90 good anti-fouling properties but more possibility for fouling and cake formation. PES control membrane has good anti-fouling and good fouling resistance. Adding nanocomposite to the membrane affects the fouling and anti-fouling properties of the membranes. PES AC and PES TiO_2 both shows the slight decline from the flux recovery (FR) and total flux ratio (Rt) than PES control. The TiO_2 and activated carbon (AC) both are hydrophobic nature, that did not affect PES membrane performance more and maintained the performance.

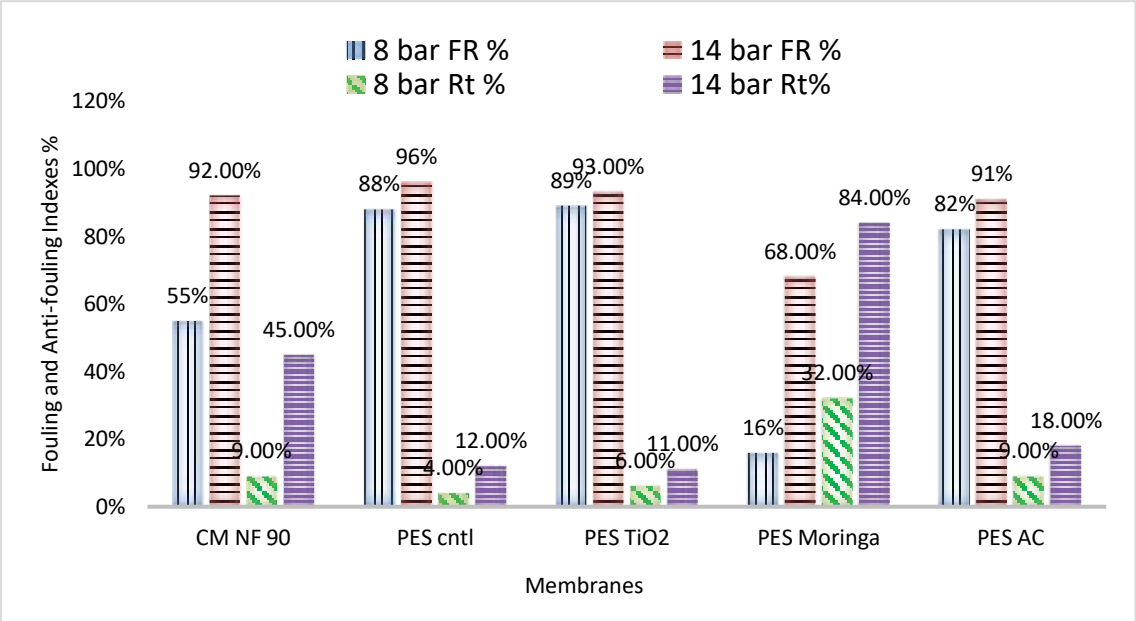

Fig. 18: Flux Recovery (FR) and Total Fouling Ratio (Rt) graph of membranes

4.7 Dye Removal Efficiency

The dye removal efficiency of the PES-based membranes was systematically examined at two operating pressures, 8 bars and 14 bars, using UV-Vis spectrophotometry. The dye selected for this study was Evans Blue, an azo compound with a peak absorbance at 607.2 nm, indicating the presence of functional groups like nitrogen and carbonyl (C=O). These membranes, enhanced with various additives, were tested to understand how pressure, time, and membrane composition influence dye removal efficiency (Shi et al. 2013). The membranes were evaluated based on their capacity to maintain removal efficiency over time (Woo et al. 2016).

From figures 19 and 20, At 8 bars pressure, all membranes showed a sharp increase in dye removal efficiency within the first 10 minutes. PES Control and PES TiO_2 showed high initial rejection rates of 92% and 97.9%, respectively. However, the PES TiO_2 membrane exhibited a slight decline over time, due to surface fouling from accumulated dye particles. PES Moringa also started with a 98% rejection but dropped to 85%, possibly due to biofouling from organic matter. PES AC membranes maintained stable performance above 92% across all time intervals, due to its large surface area and strong adsorptive capacity. The commercial CM NF90 membrane was not very effective at 8 bars, starting at 30% and slowly reaching around 90%.

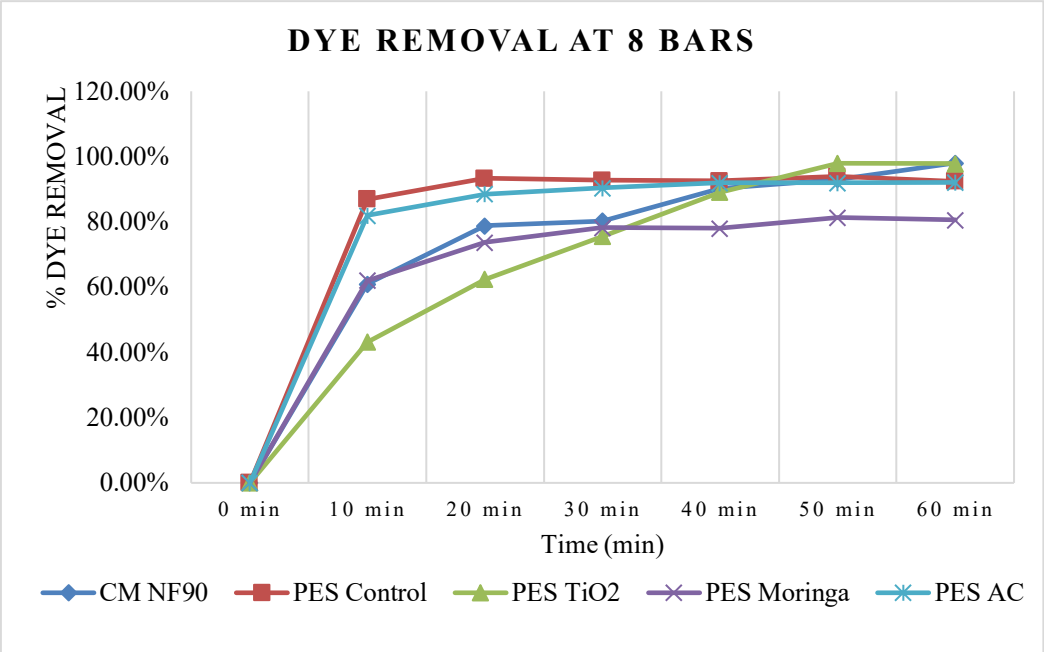

Fig.19: Graphical representation of Dye removal at 8 bars

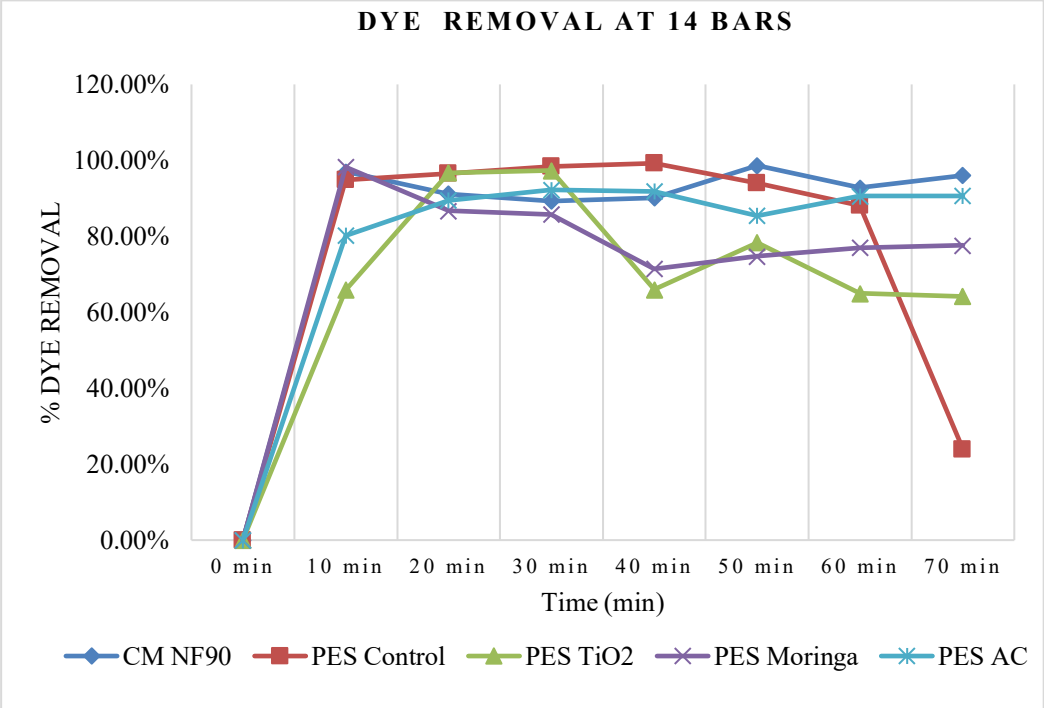

Fig.20: Graphical representation of Dye removal at 14 bars

At 14 bars, the membranes initially achieved even higher dye removal due to the increased driving force. CM NF90 efficiency significantly improved, reaching 97%, confirming its pressure-dependent nature. PES Control and PES TiO_2 again showed strong initial removal but decreased over time, with PES Control dropping dramatically to about 20% at 70 minutes. PES Moringa also exhibited a 21% decrease, due to biofouling under high-pressure conditions. PES AC maintained rejection rates between 92–95%, confirming its resistance to both organic and pressure-induced fouling.

Membranes incorporated with nanoparticles such as TiO_2 and activated carbon outperformed the unmodified PES control and the commercial NF90, particularly at lower pressures. TiO_2 helped remove dye quickly, but didn't stay as effective for long due to fouling. Activated carbon gave stable results because of its large surface area and ability to resist fouling. Moringa, a natural coagulant, improved early-stage rejection but suffered from biofouling during extended use. The importance of selecting appropriate membrane modifiers, not just for immediate efficiency but also for maintaining performance under varying pressure and operational durations.

5 Conclusion:

This study confirmed the enhanced performance of PES membranes in advancing textile wastewater treatment. The integration of titanium dioxide, activated carbon, and Moringa seed extract significantly improved PES membrane properties such as porosity, water uptake, and surface morphology, leading to enhanced dye rejection and fouling resistance. Analytical techniques like FESEM and EDS confirmed the structural integration of these additives, while FTIR and UV-Vis analyses validated their functional performance and also characterized the water uptake capacity, porosity, mean pore radius, fouling and antifouling properties. The results are summarized as, blending the green synthesized moringa, activated carbon and TiO_2 with PES polymer resulted an increase of the water uptake capacity, hydrophilicity and water flux of the control PES membrane. The nanoparticles reduced the mean pore radius of PES control and increased the porosity. The FESEM surface morphology showed that nanoparticles incorporated membranes have more aggregation, more pore clogging observed after filtration and reduced the water flux.

PES/moringa nanocomposite had the highest dye rejection (98.2%) but has more dye deposition on the pores leads to more fouling and low anti-fouling properties. Hence, the water flux declined. The PES/TiO_2 membranes achieved the highest dye rejection rate (up to 97.9%) due to increased pore formation, although their long-term efficiency was affected by fouling. while the PES/AC membranes (up to 92.2%) demonstrated consistent permeability, steady flux and strong anti-fouling properties. The membranes outperformed both the unmodified PES control and the commercial NF90 nanofiltration membrane in terms of both permeability and dye removal efficiency. Comparing with PES control, the nanoparticles blended membranes showed high water flux and flux recovery and showed excellent antifouling properties. From the findings, it is evident that selecting appropriate nanomaterials is important to balance immediate removal efficiency with long-term stability. Overall, PES-based nanocomposite membranes offer a scalable, cost-effective, and eco-friendly approach for industrial dye removal, positioning them as strong candidates for future sustainable water treatment technologies.

Author Contributions: The significant contributions of the authors were: The Membrane Preparation, data curation, interpretation, writing, and drafting: S Joy Madhumitha; The conceptualization, supervision, funding acquisition, review,

and editing: Dr.P.Jegathambal; The membrane preparation, data curation: S.Devika; The review and supervision: C Mayilswami.

Funding: The research received no external funding.

REFERENCES

[1] Aghili, F., Ghoreyshi, A.A., Rahimpour, A. and Rahimnejad, M., 2017. Coating of mixed-matrix membranes with powdered activated carbon for fouling control and treatment of dairy effluent. *Process Safety and Environmental Protection*, *107*, pp.528-539. https://doi.org/10.1016/j.psep.2017.03.013

[2] Almajras, Q.A., Hassan, A.K., Al-Juboori, R.A. and Alsalhy, Q.F., 2025. Green and sustainable biosynthesis of hybrid iron/palladium nanoparticles functionalized PES membranes for dye removal. *Desalination and Water Treatment*, *321*, p.100973. https://doi.org/10.1016/j.dwt.2024.100973

[3] AlMarzooqi, F.A., Bilad, M.R., Mansoor, B. and Arafat, H.A., 2016. A comparative study of image analysis and porometry techniques for characterization of porous membranes. *Journal of materials science*, *51*, pp.2017-2032. https://doi.org/10.1007/s10853-015-9512-0

[4] Alzain, H., Kalimugogo, V., Hussein, K. and Karkadan, M., 2023. A review of environmental impact of azo dyes. *Int J Res Rev*, *10*(6), pp.673-689. https://doi.org/10.52403/ijrr.20230682

[5] Araujo, C.S., Alves, V.N., Rezende, H.C., Almeida, I.L., de Assuncao, R.M., Tarley, C.R., Segatelli, M.G. and Coelho, N.M.M., 2010. Characterization and use of Moringa oleifera seeds as biosorbent for removing metal ions from aqueous effluents. *Water Science and Technology*, *62*(9), pp.2198-2203. https://doi.org/10.2166/wst.2010.419

[6] Bae, J., Kim, S. and Baek, S., 2022. Parallelly aligned, activated carbon coated plates operating as adsorption columns for removing VOCs. *Aerosol and Air Quality Research*, *22*(3), p.210263. https://doi.org/10.4209/aaqr.210263

[7] Benkhaya, S., M'rabet, S. and El Harfi, A., 2020. Classifications, properties, recent synthesis and applications of azo dyes. *Heliyon*, *6*(1). https://doi.org/10.1016/j.heliyon.2020.e03271

[8] Bichi, M.H., Agunwamba, J.C., Muyibi, S.A. and Abdulkarim, M.I.I., 2012. Effect of extraction method on the antimicrobial activity of Moringa oleifera seeds extract. *Journal of American science*, *8*(9), pp.450-458. http://www.jofamericanscience.org/

[9] Duan, Q., Ge, S. and Wang, C.Y., 2013. Water uptake, ionic conductivity and swelling properties of anion-exchange membrane. *Journal of Power Sources*, *243*, pp.773-778. https://doi.org/10.1016/j.jpowsour.2013.06.095

[10] Ehsani, M. and Aroujalian, A., 2020. Fabrication of electrospun polyethersulfone/titanium dioxide (PES/TiO2) composite nanofibers membrane and its application for photocatalytic degradation of phenol in aqueous solution. *Polymers for Advanced Technologies*, *31*(4), pp.772-785. https://doi.org/10.1002/pat.4813

[11] El-Sabban, H.A., Mubarak, M.F. and Diab, M.A., 2023. PPy-NTs/C/TiO2/poly (ether sulfone) porous composite membrane: Efficient ultrafiltration of Evans blue dye from industrial wastewater. *Synthetic Metals*, *297*, p.117383. https://doi.org/10.1016/j.synthmet.2023.117383

[12] Gosavi, V.D. and Sharma, S., 2014. A general review on various treatment methods for textile wastewater. *Journal of Environmental Science, Computer Science and Engineering & Technology*, *3*(1), pp.29-39

[13] Hasani-Sadrabadi, M.M., Dashtimoghadam, E., Ghaffarian, S.R., Sadrabadi, M.H.H., Heidari, M. and Moaddel, H., 2010. Novel high-performance nanocomposite proton exchange membranes based on poly (ether sulfone). *Renewable Energy*, *35*(1), pp.226-231. https://doi.org/10.1016/j.renene.2009.05.026

[14] Hasheesh, M., El-Kashif, E.F., Mohamed, A. and Saood, M., 2024. The effect of activated carbon nanoparticles (ACNPs) on characterization and mechanical properties of polyethersulfone (PES) ultrafiltration membranes. *Polymer Bulletin*, *81*(16), pp.14855-14874. https://doi.org/10.1007/s00289-024-05399-3

[15] Ho, R.W.J., 2023. *Development of quaternary system pes polymeric hybrid membranes with blending method: study on the effect of powdered activated carbon and nanosilica* (Doctoral dissertation, UTAR). http://eprints.utar.edu.my/id/eprint/5707

[16] Hossain, L., Sarker, S.K. and Khan, M.S., 2018. Evaluation of present and future wastewater impacts of textile dyeing industries in Bangladesh. *Environmental Development*, *26*, pp.23-33. https://doi.org/10.1016/j.envdev.2018.03.005

[17] Jahan, I.A., Hossain, M.H., Ahmed, K.S., Sultana, Z., Biswas, P.K. and Nada, K., 2018. Antioxidant activity of Moringa oleifera seed extracts. *Oriental Pharmacy and Experimental Medicine*, *18*, pp.299-307. https://doi.org/10.1007/s13596-018-0333-y

[18] Jayabalakrishnan, S.S., Selvasekarapandian, S., Aafrin Hazaana, S., Kavitha, P. and Vengadesh Krishna, M., 2023. Proton-conducting Moringa oleifera seed-based biomaterial electrolyte for electrochemical applications. *Ionics*, *29*(1), pp.331-344. https://doi.org/10.1007/s11581-022-04797-9

[19] Kim, Y.H., Eom, J.Y., Kim, K.Y., Lee, Y.S., Kim, H.S. and Hwang, S.J., 2010. Applicability study of backwash water treatment using tubular membrane system with dead-end filtration operation mode. *Desalination*, *261*(1-2), pp.104-110. https://doi.org/10.1016/j.desal.2010.05.023

[20] Lincy, A., Jegathambal, P., Mkandawire, M. and MacQuarrie, S., 2020. Nano bioremediation of textile dye effluent using magnetite nanoparticles encapsulated alginate beads. *J. Environ. Treat. Tech*, *8*(3), pp.936-946. http://www.jett.dormaj.com/

[21] Li, N., Wang, X., Zhang, H., Zhang, Z., Ding, J. and Lu, J., 2019. Comparing the performance of various nanofiltration membranes in advanced oxidation-nanofiltration treatment of reverse osmosis concentrates. *Environmental Science and Pollution Research*, *26*, pp.17472-17481. https://doi.org/10.1007/s11356-019-05120-2

[22] Liu, L., Cheng, R., Chen, X., Zheng, X., Shi, L., Cao, D. and Zhang, Z., 2017. Applications of membrane technology in treating wastewater from the dyeing industry in China: Current status and prospect. *Desalination and Water Treatment*, *77*, pp.366-376. https://doi.org/10.5004/dwt.2017.20775

[23] Madhumitha, S. Joy, A. Gracy, and M. Balaji. "Dye effluent treatment using activated coconut shell charcoal compared with zeolite filter." *AIP Conference Proceedings*. Vol. 2912. No. 1. AIP Publishing, 2023. https://doi.org/10.1063/5.0170769

[24] Moradihamedani, P., 2022. Recent advances in dye removal from wastewater by membrane technology: a review. *Polymer Bulletin*, *79*(4), pp.2603-2631. https://doi.org/10.1007/s00289-021-03603-2

[25] Nisha, R.R., Jegathambal, P., Parameswari, K. and Kirupa, K., 2017. Biocompatible water softening system using cationic protein from moringa oleifera extract. *Applied Water Science*, *7*, pp.2933-2941. https://doi.org/10.1007/s13201-017-0591-8

[26] Rahimpour, A., Madaeni, S.S., Taheri, A.H. and Mansourpanah, Y., 2008. Coupling TiO2 nanoparticles with UV irradiation for modification of polyethersulfone ultrafiltration membranes. *Journal of Membrane Science*, *313*(1-2), pp.158-169. https://doi.org/10.1016/j.memsci.2007.12.075

[27] Safarpour, M., Vatanpour, V. and Khataee, A., 2016. Preparation and characterization of graphene oxide/TiO2 blended PES nanofiltration membrane with improved antifouling and separation performance. *Desalination*, *393*, pp.65-78. https://doi.org/10.1016/j.desal.2015.07.003

[28] She, F.H., Tung, K.L. and Kong, L.X., 2008. Calculation of effective pore diameters in porous filtration membranes with image analysis. *Robotics and Computer-Integrated Manufacturing*, *24*(3), pp.427-434. https://doi.org/10.1016/j.rcim.2007.02.023

[29] Shi, H., Magaye, R., Castranova, V. and Zhao, J., 2013. Titanium dioxide nanoparticles: a review of current toxicological data. *Particle and fibre toxicology*, *10*, pp.1-33. https://doi.org/10.1186/1743-8977-10-15

[30] Stawade BV, apata IE, pradhan N, karim A, raghavan D. Recent advances in the synthesis of polymer-grafted low-k and high-k nanoparticles for dielectric and electronic applications. *Molecules*. 2021; 26(10):2942. Https://doi.Org/10.3390/molecules26102942 Surface modified membranes.

[31] Thamaraiselvan, C. and Noel, M., 2015. Membrane processes for dye wastewater treatment: recent progress in fouling control. *Critical Reviews in Environmental Science and Technology*, *45*(10), pp.1007-1040. https://doi.org/10.1080/10643389.2014.900242

[32] Vatanpour, V., Madaeni, S.S., Khataee, A.R., Salehi, E., Zinadini, S. and Monfared, H.A., 2012. TiO2 embedded mixed matrix PES nanocomposite membranes: Influence of different sizes and types of nanoparticles on antifouling and performance. *Desalination*, *292*, pp.19-29.

[33] Vergis, B.R., Kottam, N., Krishna, R.H. and Nagabhushana, B.M., 2019. Removal of Evans Blue dye from aqueous solution using magnetic spinel ZnFe2O4 nanomaterial: Adsorption isotherms and kinetics. *Nano-structures & Nano-objects*, *18*, p.100290. https://doi.org/10.1016/j.nanoso.2019.100290

[34] Woo, Y.C., Lee, J.J., Shim, W.G., Shon, H.K., Tijing, L.D., Yao, M. and Kim, H.S., 2016. Effect of powdered activated carbon on integrated submerged membrane bioreactor–nanofiltration process for wastewater reclamation. *Bioresource Technology*, *210*, pp.18-25. https://doi.org/10.1016/j.biortech.2016.02.023

[35] Wooddell, C.I., Radley-Crabb, H.G., Griffin, J.B. and Zhang, G., 2011. Myofiber damage evaluation by Evans blue dye injection. *Current Protocols in Mouse Biology*, *1*(4), pp.463-488. https://doi.org/10.1002/9780470942390.mo110141

[36] Wu, T., Zhang, Z., Zhai, D., Liu, Y., Liu, Q., Xue, L. and Gao, C., 2019. Dye degrading and fouling-resistant membranes formed by deposition with ternary nanocomposites of N-doped graphene/TiO2/activated carbon. *Membranes*, *9*(1), p.16

[37] Xu, Z.L. and Qusay, F.A., 2004. Polyethersulfone (PES) hollow fiber ultrafiltration membranes prepared by PES/non-solvent/NMP solution. *Journal of Membrane Science*, *233*(1-2), pp.101-111. https://doi.org/10.1016/j.memsci.2004.01.005

[38] Yam-Cervantes, M.A., Sulub-Sulub, R., Hunh-Ibarra, M., Duarte, S., Uc-Fernandez, E., Pérez-Canales, D., Aguilar-Vega, M. and González-Díaz, M.O., 2024. Asymmetric Membranes Obtained from Sulfonated HIPS Waste with Potential Application in Wastewater Treatment. *Membranes*, *14*(12), p.247. https://doi.org/10.3390/membranes14120247

[39] Yao, L., Xue, X., Yu, P., Ni, Y. and Chen, F., 2018. Evans blue dye: a revisit of its applications in biomedicine. *Contrast media & molecular imaging*, *2018*(1), p.7628037. https://doi.org/10.1155/2018/7628037